

Tissue hydraulics: physics of lumen formation and interaction

Alejandro Torres-Sánchez,^{1,*} Max Kerr Winter,^{1,*} and Guillaume Salbreux^{1,2,†}

¹The Francis Crick Institute, 1 Midland Road, NW1 1AT, United Kingdom

²University of Geneva, Quai Ernest Ansermet 30, 1205 Genève, Switzerland

(Dated: October 7, 2022)

Lumen formation plays an essential role in the morphogenesis of tissues during development. Here we review the physical principles that play a role in the growth and coarsening of lumens. Solute pumping by the cell, hydraulic flows driven by differences of osmotic and hydrostatic pressures, balance of forces between extracellular fluids and cell-generated cytoskeletal forces, and electro-osmotic effects have been implicated in determining the dynamics and steady-state of lumens. We use the framework of linear irreversible thermodynamics to discuss the relevant force, time and length scales involved in these processes. We focus on order of magnitude estimates of physical parameters controlling lumen formation and coarsening.

Lumen formation is ubiquitous in developmental biology [1–5]. The successful opening of fluid filled spaces within tissues is crucial for a zygote to grow into a topologically complex adult organism containing multiple cavities and networks of tubes. There are many prominent examples of lumen formation in development [3], and before turning to the physics of lumen formation and their interactions, we first discuss here some of these examples, illustrating the variety of roles lumen formation plays by contributing to morphogenesis, symmetry breaking, cell fate specification, or size control.

Lumen expansion driven by fluid flow, which is the essential process we discuss here, is one the fundamental mechanisms by which lumens can form [3]. We review the physics of this process in more detail in section I. Fluid accumulation has been implicated or proposed to participate e.g. in zebrafish gut formation [6], neural tube expansion [7], brain ventricular expansion [8], otic vesicle formation [9], formation of Kupffer vesicle [10] or in the developing mouse salivary gland [11]. During embryogenesis, fluid pumping by polarised cells in the epiblast, rather than cell apoptosis, acts as a lumen formation mechanism in the mouse pro-amniotic cavity [12]. The prospective pro-amniotic cavity forms in a similar way in the epiblast of human embryos, where a lumen opens in the centre of a rosette of polarised cells, and in the absence of apoptosis [13].

Larger lumens form in some cases through the coarsening of smaller lumens; we discuss this process in more detail in section II. In the zebrafish gut, multiple small lumens open via fluid accumulation driven by paracellular ion transport [6, 14]. These lumens subsequently fuse by tissue remodelling where cell-cell adhesions are lost in the tissue bridges separating neighbouring lumens. Fusion is a distinct process to lumen nucleation, as demonstrated by *smoothened* mutants that exhibit small lumens which fail to fuse [6, 14]. A similar coarsening mechanism has

also been reported during the formation of the blastocyst, the first lumen forming event in both mouse and human development [9, 15–18]. The successful formation of the blastocyst is crucial for the viability of the embryo [19] and occurs by the active pumping of fluid into the centre of the embryo by an outer layer of polarised cells. Initially, a large number of microlumens form in the intercellular space by hydraulic fracturing of cell-cell adhesions. Then, these combine into a single, large lumen (see Fig. 1a, where Dextran fluid labelling allows to visualise the transient fluid accumulation at cell-cell contacts [9]). The opening of the blastocoel breaks the spherical symmetry of the embryo, isolating a group of cells, the inner cell mass, which goes on to form the body of the organism. As such, this is an example of lumen formation acting as a patterning event [20].

The interplay of luminal pressure and the rupture and healing dynamics of the surrounding epithelium has been proposed to act as a size control mechanism. In the mouse blastocyst, increased luminal pressure leads to increased tension in the trophectoderm, the epithelium lining the blastocoel. Above a critical tension, cell-cell adhesions cannot be maintained during mitosis, resulting in the temporary rupture of the blastocyst. This mechanism results in the cavity radius oscillating about some average value [24], following a mechanism which had also been proposed to explain tissue oscillations observed during *Hydra* regeneration [25]. These oscillations have been modelled by considering a spherical elastic shell surrounding a pressurised lumen, which ruptures with a circular tear above a critical surface tension. Following rupture, luminal fluid flows out of the tear, the tension decreases, and the tear heals at some lower tension. Denoting σ_c and σ_h the surface tensions at which the tear opens and closes, E the 2D elastic modulus of the epithelium, and assuming $|\sigma_c - \sigma_h| \ll E$, this process results in oscillations around a mean radius value for the lumen $R \sim R_0(1 + \sigma_c/E)$ with R_0 the radius without tension, and amplitude $\Delta R \sim (\sigma_c - \sigma_h)/E$ [26]. Luminal pressure has also been studied, and directly measured, in the developing zebrafish inner ear [27, 28]. Here it has been proposed that hydrostatic pressure arising from

*Equal contribution

†To whom correspondence should be addressed: guillaume.salbreux@unige.ch

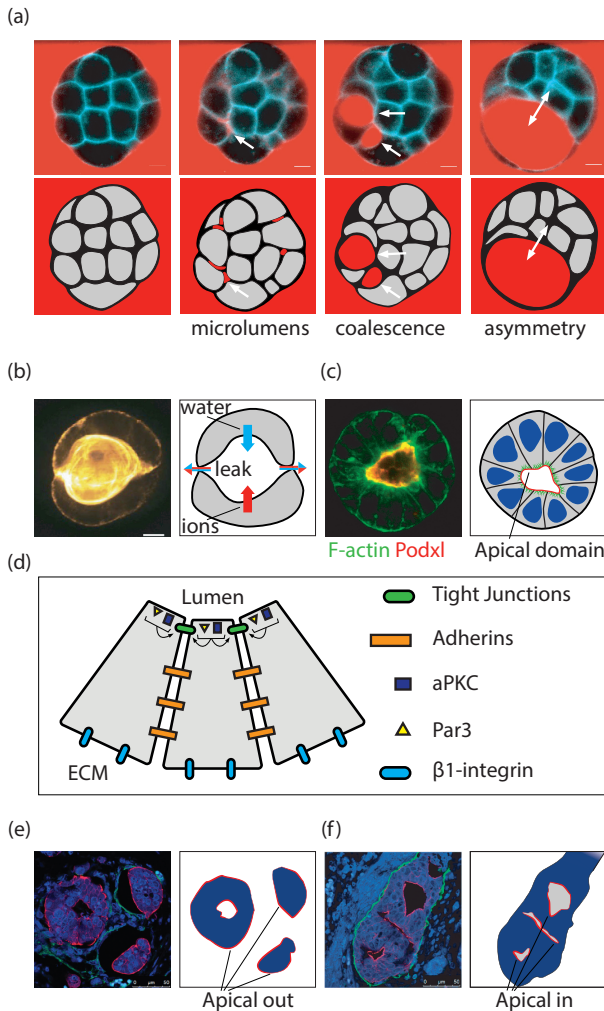


FIG. 1: Examples of lumen formation. (a) Formation of the mouse blastocyst. The surrounding fluid is pumped into the centre of the embryo, forming microlumens. These microlumens then coalesce, and eventually form one large lumen, the blastocoel. This event breaks the spherical symmetry of the embryo. Top images: cyan, plasma membrane label; red, Dextran; Scale bar, 10 μ m [9]. (b) A lumen formed between two rat hepatocytes. This process has been modelled as a balance between active pumping into the cavity, and paracellular leakage out of it [21]. (c) A spherical aggregate of mouse epiblast stem cells. The anti-adhesive molecule podocalyxin (Podxl) is expressed at the apical domain. Aggregates of epiblast cells recapitulate lumen forming events in the mouse embryo (image courtesy of M. Shahbazi). (d) A schematic of the polarised structure of epithelial cells surrounding a lumen. The basal domain is established by sensing the external environment via β 1-integrins [22]. Tight junctions form on the apicolateral interfaces. The apical domain is characterised by apical proteins such as aPKC and PAR3. (e), (f) Colorectal cancer samples demonstrating apical polarity directed outward (e) and inward (f) [23]. All images are reproduced with permission.

stresses developing in the epithelium can act as a correcting size mechanism: indeed a decrease in size of the otic vesicle results in stress relaxation in the epithelium, lowering the hydrostatic pressure in the lumen and leading to faster growth [28]. On a smaller scale, lumen expansion has been associated during zebrafish sprouting angiogenesis with pressure-driven inverse membrane blebbing, local membrane protrusions resulting from membrane/cortex detachment [29].

In the developing mouse aorta, a vascular lumen is initiated at cellular interfaces between endothelial cells [38]. It has been suggested that repulsion of negatively charged tissue interfaces contribute to this lumen formation process [39]. Such repulsive interactions are thought to be due to charged “anti-adhesin” molecules at the cell surface, such as podocalyxin, which can be secreted into the lumen nucleation site, with electrostatic forces separating adhering cells. Podocalyxin is a transmembrane protein and a constituent of the glycocalyx whose “anti-adhesive” effect has been documented e.g. through its effect in decreasing cell aggregation in MDCK cells [40] and has been shown to be dependent on sialic acid [41]. Since electric charges are screened on short distances of \sim nm in electrolyte solutions, physical arguments indicate that such electrostatic repulsive interactions occur if cells, or their glycocalyx layer, are in very close contact. We give in the box “Interaction of charged surfaces” order of magnitude estimates of the interaction of charged plates to illustrate this discussion. Podocalyxin might also have a more indirect effect on cell adhesion, as it has also been shown to promote the formation of microvilli at the cell surface [42].

As well as physically separating groups of cells, lumens contribute to patterning by the presence of signalling molecules in the luminal fluid, accumulating in microlumens [43]. These microlumens can act as signalling hubs, as secreted diffusible molecules can easily reach cells enclosing the lumen, ensuring their coordinated response. During mouse blastocyst formation, the specification and segregation of the epiblast and primitive endoderm, with the latter being eventually in contact with the lumen, occurs concomitantly with lumen expansion and is impaired if lumen expansion does not proceed normally [44].

In vitro systems allow the mechanisms of lumen formation to be studied in isolation. An example of such an isolated lumen forming between two rat hepatocytes is shown in Fig. 1b. This process of lumen formation has been described theoretically with a model involving the balance of fluid pumping by the cells into the lumen with paracellular leakage out of it [21]. Hepatocytes have also been used to study the formation of anisotropic lumens which do not assume a spherical shape and can have a biased position along cellular interfaces [45].

Madin-Darby Canine Kidney (MDCK) cells are a common model *in vitro* system for studying lumen formation, as they readily self-organise into polarised epithelial spheres surrounding a lumen when grown in 3D [46] and can form with opposite polarities when grown in suspen-

Interaction of charged surfaces. Here we discuss the physics of the interaction of charged surfaces in an electrolyte solution. We consider an electrolyte solution with 1:1 charge ratio and valence z (e.g. NaCl, with $z = 1$). The steady-state concentration profile of ionic species is described for small electric potential by the linearised Poisson-Boltzmann equation [30],

$$\nabla^2 \phi = \frac{2\bar{c}z^2 e^2}{\epsilon kT} \phi = \frac{1}{\ell_{\text{DH}}^2} \phi, \quad (1)$$

where ϵ is the dielectric permittivity of the solvent, e the charge of an electron, \bar{c} the background concentration of electrolyte, k the Boltzmann constant, T the temperature, and ϕ the electric potential. We have also introduced the Debye-Hückel screening length $\ell_{\text{DH}} = \sqrt{\epsilon kT / (2\bar{c}z^2 e^2)}$, which determines the length scale on which electrostatic interactions can occur in an electrolyte solution. Substituting in a typical biological concentration of Na^+ , Cl^- $c_0 \sim 100$ mM [30], $z = 1$, $e = 1.6 \times 10^{-19}$ C, $\epsilon = \epsilon_r \epsilon_0 \approx 74.5 \epsilon_0 \approx 7 \times 10^{-10}$ F/m with ϵ_0 the vacuum permittivity and ϵ_r the relative permittivity of water [31], and $kT = 4 \times 10^{-21}$ J, we get $\ell_{\text{DH}} \approx 1$ nm. For comparison, the typical length of a E-cadherin junction is 25 nm [32]. Contact repulsion through negative charges would therefore have to occur on very close contact between cellular interfaces.

How strong can the force from such a repulsive contact be? The pressure acting on two charged planar interfaces separated by a distance d and carrying a charge per unit area en is, for small electric potentials [30]:

$$P = \frac{2e^2 n^2}{\epsilon} \exp\left(-\frac{d}{\ell_{\text{DH}}}\right). \quad (2)$$

The rupture force of a single cadherin bond is of the order of 100pN [33]. Approximately 400 cadherin dimers span a cell-cell interface of area $100\mu\text{m}^2$ (taking a cadherin density of 80 molecules/ μm^2 , with a ratio of monomers to dimers of 17:1 [34]), giving a rupture pressure of ~ 400 Pa. According to Eq. (2), the charge density required to generate a repulsive pressure leading to cadherin rupture is $3 \times 10^3 \mu\text{m}^{-2} < n < 6 \times 10^8 \mu\text{m}^{-2}$ for distances d ranging between 0 and 25nm. The charge of podocalyxin is approximately -16e, and is supplemented by approximately 20 sialic acid molecules, each of which carries a charge of $-e$ [35–37]. Consequently, these charge densities correspond to between 200 and 4×10^7 podocalyxin molecules in the interface. A lower bound of podocalyxin density on rat epithelial cells of $20\mu\text{m}^{-2}$ has been reported [36], corresponding to 2000 molecules on a $100\mu\text{m}^2$ interface. We conclude that repulsive electrostatic forces could be high enough to separate cell membranes, but the corresponding forces can only act at very short distance. This analysis is however highly simplified, as notably the size of charged membrane protein is not small compared to the Debye length.

sion or in collagen gels [47]. In cysts formed in collagen gels, the apical side is facing the lumen, and apicobasal polarity in MDCK cells is initiated by the sensing of collagen in the extra-cellular matrix (ECM) via $\beta 1$ -integrins [48]. This signal induces reorganisation of the cytoskeleton, and the accumulation of apical polarity proteins, such as aPKC and Par3, at a region of the inward facing cell membrane called the apical membrane initiation site [2, 49, 50]. This is shown schematically in Fig. 1d. Having established an inward facing apical domain, the lumen begins to form by active pumping. As well as in spherical cysts, the mechanics and hydraulics of MDCK cells have long been studied in doming epithelial monolayers, which form local blisters by detachment from the substrate [51–53]. Blisters are hydraulically connected through the lateral intercellular space (LIS), which is compliant to hydrostatic pressure, or through flows occurring basally [54]. When the epithelium is subjected to a sudden increase of basal hydrostatic pressure [55], hydraulic fractures appear in the LIS which are reminiscent of the microlumens forming in the mouse embryo [9]. Recently, epithelial blisters have been employed to demonstrate the ability of the epithelium to sustain large deformations at constant tension, a hallmark of superelasticity [56].

Recent experiments have demonstrated the extent to which embryonic stem cells can self-organise [57–59]. Aggregates of a single stem cell lineage, epiblast cells,

have been studied *in vitro*, with a particular emphasis on their ability to form lumens [12] (Fig. 1c). Similar to MDCK aggregates, an internal apical domain is established through a mechanism which is dependent on $\beta 1$ -integrin signaling [12, 60]. In both mouse and human cells, successful lumen formation is coordinated by the transition from naive to primed pluripotent states. As cells exit naive pluripotency the transcription factor OCT4 is activated, which in turn results in the expression of podocalyxin, and ultimately lumen nucleation [61].

Outside of developmental biology, the formation, maintenance or disruption of lumens play a role in polycystic kidney disease and cancer. In polycystic kidney disease, the renal epithelial tubules are abnormally enlarged, and ions pumps and transporters are mislocalized at the apical and basal interfaces of the epithelium [62]. Cancerous cells can disrupt normal tissue organisation in mammary glands by a process called luminal filling, associated with a loss of the luminal space [63, 64]. Conversely, several cancerous cell types, when cultured *in vitro*, spontaneously self-organise in a spheroid surrounding a single or multiple lumens, e.g. cancerous breast cells [65] or colorectal cancer cells [66]. Colorectal tumours also form multiple lumens surrounded by polarised epithelia *in vivo*; interestingly these spheroids can form with their apico-basal polarity oriented either towards or away from the central lumen [23] (Fig. 1e-f).

Due to the fundamental physical mechanisms at play

in lumen formation, these topics have attracted considerable attention within the biophysics community. In the next sections, we discuss some of the biophysical processes involved in lumen formation and interactions.

I. TISSUE PUMPING AND THE GROWTH OF SINGLE LUMEN

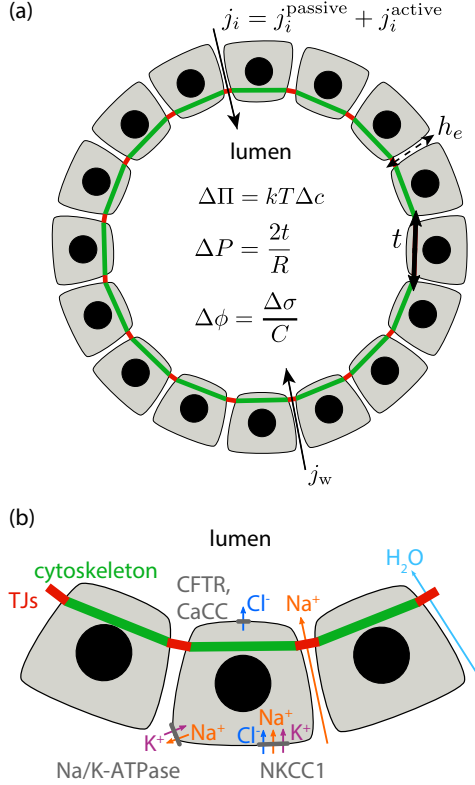


FIG. 2: Mechanisms of lumen formation. (a) Water flows in the lumen due to a difference in osmotic pressure and hydrostatic pressures $\Delta\Pi - \Delta P$, and possibly through electro-osmotic effects. The hydrostatic pressure in a spherical lumen of radius R is related to the tension t in the monolayer through Laplace’s law. The difference in osmotic pressure is maintained by the active transport of ions, which can also lead to a difference in electrostatic potential $\Delta\phi$. (b) Mechanisms of active ion transport. The active transport of Na^+ in the basolateral side leads to a secondary active transport of Cl^- , which is exported to the lumen. In leaky epithelia, some ions, such as Na^+ , flow through the intercellular space, in the paracellular domain, to balance the excess of negative charge in the lumen.

To discuss the different mechanisms by which water can be passively transported across an epithelium, here we follow the framework of linear irreversible thermodynamics. In this framework, molecular fluxes are proportional to the chemical potential differences across the layer, with proportionality coefficients characterising the different couplings in the system [67, 68]. In the Box

“Passive flux of water and ions across a layer” we give further details about the corresponding derivation, including the expression for the chemical potential of water and solutes. Assuming a dilute solution of N ion types with concentrations c_i and charges q_i , the flux of water is given by the expression

$$j_w = \lambda_w (\Delta\Pi - \Delta P) - \sum_{i=1}^N \lambda_{w,i} \left(\Delta c_i + \frac{q_i \bar{c}_i}{kT} \Delta\phi \right) + j_w^{\text{active}}, \quad (3)$$

where Δc_i is the difference of concentration across the layer, i.e. $\Delta c_i = c_i^l - c_i^o$ with c_i^l the concentration in the lumen and c_i^o the concentration outside, $\bar{c}_i = (c_i^l + c_i^o)/2$ is the average concentration, $\Delta\Pi = kT \sum_{i=1}^N \Delta c_i$ is the osmotic pressure difference, $\Delta\phi$ the difference in electric potential, ΔP is the hydrostatic pressure difference, λ_w is the permeability of the layer to water and $\lambda_{w,i}$ is a cross-coupling coefficient characterising the flow of water that is driven by differences of solute chemical potential across the epithelium (Fig. 2a). The flux j_w is given in units of a permeation velocity. In the right-hand side of Eq. 3, the first two terms correspond to passive water flows due to differences in its chemical potential and to dissipative couplings with other molecules in the solution, either in the form of passive dragging [69] or through cotransport via symporters [70]. In the last term, we have also included a possible active contribution to water pumping. We are not aware of a known active mechanism of cellular water transport; we note however that apico-basal actomyosin cortical flows, for instance, could in principle bring such an active contribution, from friction forces between the extracellular fluid and the cortical cytoskeleton.

The flux of solutes is given by

$$j_i = -\lambda_i \left(\Delta c_i + \frac{q_i \bar{c}_i}{kT} \Delta\phi \right) + \lambda_{i,w} (\Delta\Pi - \Delta P) - \sum_{j \neq i} \lambda_{i,j} \left(\Delta c_j + \frac{q_j \bar{c}_j}{kT} \Delta\phi \right) + j_i^{\text{active}}, \quad (4)$$

where λ_i is the permeability of the layer to solute i , and $\lambda_{i,w}$, $\lambda_{i,j}$ are cross-coupling coefficients characterising the flow of solute that is driven by differences of chemical potential of water and other solutes, across the epithelium. Here j_i has the usual units of a flux density, i.e. number of particles per unit area and time. As for the water flux, in the right-hand side of Eq. 4, the first three terms describe passive fluxes of solutes, while the last term describes active solute pumping by the epithelium. The coefficients λ_w , λ_i , $\lambda_{w,i}$, $\lambda_{i,j}$ form the matrix of phenomenological coefficients and encode all possible passive interactions between molecules across the layer. We now look at the interpretation of these parameters based on previous studies.

The epithelial permeability to water is characterised by λ_w and encodes the effective permeability to both paracellular flows across the LIS and transcellular flows occurring across the lipid membrane or aquaporins.

Passive flux of water and ions across an epithelial layer. Here we discuss the equations determining the flux of water and ions across a layer following the framework of irreversible thermodynamics. We consider the free energy density of a solution of N ion types in water

$$f(c_w, \{c_i\}_i^N) = \mu_w^{\text{ref}} c_w + kT c_w \log \left(\frac{c_w}{c_w + \sum_{i=1}^N c_i} \right) + kT \sum_{i=1}^N c_i \left[\mu_i^{\text{ref}} + \log \left(\frac{c_i}{c_w + \sum_{i=1}^N c_i} \right) + q_i \Phi \right], \quad (5)$$

where c_w is the concentration of water, μ_w^{ref} its reference chemical potential, c_i is the concentration of the i -th solute, q_i its charge, μ_i^{ref} its reference chemical potential, and Φ is the electric potential. The second and third terms in the right-hand side of Eq. 5 are respectively the entropy density of mixing and the potential energy of charges in solution. The Gibbs free energy density is then given by $g(c_w, \{c_i\}_i^N, P) = f(c_w, \{c_i\}_i^N) + P(c_w v_w + \sum_{i=1}^N c_i v_i)$ with P the pressure in the system. The chemical potentials are given by

$$\mu_w = \frac{\partial g}{\partial c_w} \approx \mu_w^{\text{ref}} + v_w \left(P - kT \sum_{i=1}^N c_i \right), \quad (6)$$

$$\mu_i = \frac{\partial g}{\partial c_i} \approx \mu_i^{\text{ref}} + kT \log c_i + q_i \Phi + P v_i, \quad (7)$$

where in the last expressions we have written the leading order terms for a dilute, incompressible mixture in which $c_i/c_w \ll 1$ and $c_w v_w + \sum_{i=1}^N c_i v_i = 1$. The passive flux density across the epithelial monolayer of water, j_w , and ions j_i , will then follow the gradient of their chemical potentials. Following the framework of linear irreversible thermodynamics [68], we have that

$$\begin{pmatrix} \hat{j}_w \\ \hat{j}_1 \\ \vdots \\ \hat{j}_N \end{pmatrix} = - \begin{pmatrix} \bar{\lambda}_w & \bar{\lambda}_{w1} & \cdots & \bar{\lambda}_{wN} \\ \bar{\lambda}_{w1} & \bar{\lambda}_1 & \cdots & \bar{\lambda}_{1N} \\ \vdots & \vdots & \ddots & \vdots \\ \bar{\lambda}_{wN} & \bar{\lambda}_{1N} & \cdots & \bar{\lambda}_N \end{pmatrix} \begin{pmatrix} \Delta \mu_w \\ \Delta \mu_1 \\ \vdots \\ \Delta \mu_N \end{pmatrix}, \quad (8)$$

where the matrix is the symmetric and positive semidefinite matrix of Onsager coefficients. To get Eqs. (3) and (4), we define the permeation velocity of water in terms of its flux density as $j_w = \hat{j}_w v_w$. For the chemical potential of ions, we expand

$$\Delta \mu_i \approx \left[kT \frac{\Delta c_i}{\bar{c}_i} + q_i \Delta \phi + \Delta P v_i \right], \quad (9)$$

where, taking into account that $kT/v_i \sim 100$ kPa, and since a typical excess pressure in the lumen is $\Delta P \sim 0.1$ kPa [56], we assume that the last term can be neglected. Finally we define the parameters $\lambda_w = \bar{\lambda}_w v_w^2$, $\lambda_i = \bar{\lambda}_i kT/\bar{c}_i$, $\lambda_{i,j} = \bar{\lambda}_{ij} kT/\bar{c}_j$, $\lambda_{w,i} = \bar{\lambda}_{wi} kT v_w/\bar{c}_i$ and $\lambda_{i,w} = \bar{\lambda}_{wi} v_w$.

For MDCK cells $\lambda_w \sim (0.1 - 1) \cdot 10^{-7} \mu\text{m}\cdot\text{s}^{-1}\cdot\text{Pa}^{-1}$ [54, 56]. This number is comparable to typical values of lipid membranes water permeabilities $\lambda_m \sim 0.7 \times 10^{-7} \mu\text{m}\cdot\text{s}^{-1}\cdot\text{Pa}^{-1}$ (corresponding to a membrane permeability coefficient $P_f = 10 \mu\text{m}\cdot\text{s}^{-1}$ [71]). Higher values have been reported for other epithelia ($\sim 70 - 100$ times larger for the gallbladder and for the kidney proximal tubule [72]). During growth of the zebrafish inner ear, the water flux j_w is of the order of $1 - 8 \mu\text{m}/\text{h}$ [28]; corresponding with the reported values of λ_w , using Eq. (3) and neglecting cross-coupling coefficients, to a driving pressure difference $\Delta \Pi - \Delta P \sim 3 - 200$ kPa. This relatively high pressure difference, compared to typical cytoskeletal pressures of ~ 100 Pa [73], is however consistent with physiological osmotic pressure differences: using Van't Hoff law, a difference of concentration of $1 - 100$ mM across the epithelium yields an osmotic pressure difference $\Delta \Pi \sim 2.6 - 260$ kPa. Direct pressure measurements of the intraluminal pressure in the growing zebrafish otic vesicle, using a sensor coupled to a glass needle penetrating into the vesicle, indicate lower values for the excess pressure ΔP of the order of $100 - 300$ Pa [28]; similar values for ΔP are found in the blastocoel ($\Delta P \sim 250$

Pa) [9], in epithelial domes ($\Delta P \sim 100$ Pa) [56], and in MDCK cysts ($\Delta P \sim 40$ Pa [74] which was found to decrease to ~ 20 Pa following inhibition of the CFTR channel). These observations suggest that a mode of lumen growth which occurs in the regime $\Delta \Pi \gg \Delta P$. We also note that the difference of pressure ΔP in Eq. (3) is not necessarily constant, and in particular dissipative processes associated to tissue deformation might also contribute to ΔP and further slow down, or entirely control, the speed of lumen expansion. Considering the epithelium as a purely fluid layer with two-dimensional viscosity η , one would have $\Delta P = (2\eta/R^2)dR/dt$. Plugging this relation in Eq. (10) indicates that the relative role of tissue viscosity and fluid permeation in controlling the speed of lumen expansion is set by the dimensionless ratio $2\lambda_w \eta/R^2$. With a typical 3D tissue viscosity $\eta_{3D} \sim 10^5 - 10^6$ Pa.s [75, 76], $\eta \sim h\eta_{3D}$ with $h \sim 10 \mu\text{m}$ the tissue thickness and $R \sim 100 \mu\text{m}$, one obtains $2\lambda_w \eta/R^2 \sim 2 \times 10^{-4} - 10^{-6}$, indicating that in general water permeation is the dominating dissipative process.

The epithelial ion permeability, relating the ion flux density across the layer to a gradient in its chemical potential, is characterised by λ_i and, as well as λ_w , it ef-

fectively encodes the permeability for both paracellular and transcellular fluxes, including the effect of ion channels, pores, carriers and symporters. This permeability however excludes the effect of pumps: pumps are indeed actively transporting ions by consuming a source of chemical energy such as ATP; we will discuss them later. The paracellular ion permeability depends on the permeability of tight junctions, some of which can be cation/anion selective [77]. For instance, tight MDCK monolayers, which are devoid of claudin-2 TJ proteins that facilitate the permeation of small cations such as Na^+ or K^+ , develop very large transepithelial potentials and very large electric resistance $\sim 10 \text{ k}\Omega\text{cm}^2$. When transfected with claudin-2-cDNA, the resistance lowers to $150\text{-}500 \text{ }\Omega\text{cm}^2$ [78]. Measures of λ_i are scarce in the literature but an order of magnitude can be obtained from measurements of epithelial electric resistance [21]. Given that $q_i j_i$ is an electric current, $\omega_i = kT/(\lambda_i \bar{c}_i^2)$ is an electric resistance times unit area, which for epithelial monolayers is typically in the range $10 - 1000 \text{ }\Omega\cdot\text{cm}^2$ [79]. Using typical ion concentrations of 100 mM [30] and $q_i = e$ the electron charge, we can obtain an estimate for the permeability $\lambda_i = 3 \times 10^{-2} - 3 \text{ }\mu\text{m/s}$, in agreement with the permeability of Na^+ in MDCK monolayers $\lambda_i = 1.7 \times 10^{-1} \text{ }\mu\text{m/s}$ [53]. If one imposes a difference in solute concentration across the epithelium, and assuming a vanishing difference of hydrostatic pressure, both a water flux and a solute flux results from this difference. The relative magnitude between these resulting water and ion fluxes is controlled by the dimensionless ratio $kT\bar{c}_i\lambda_w/\lambda_i = 10^{-3} - 1$, which indicates that water permeation speed is comparable to or slower than ion exchange. This indicates that to maintain a difference of osmotic pressure across the epithelium, either the ion permeability λ_i is actually lower for some species, or active fluxes must constantly compensate for ion leakage, as we discuss below.

In leaky epithelia, with a low electric resistance, the difference of electric potential across the epithelium is small $\Delta\phi \approx 0$ [80]. However, tight epithelia can maintain high values of transepithelial potential ($\Delta\phi \sim \pm 50 \text{ mV}$) [79]. Some lumen, such as the vestibular endolymph [81] or the bladder [82], require a tight control of their transepithelial potential for their proper function. Denoting C the capacitance per unit area of the epithelium (with order of magnitude $C \sim 10^{-2} \text{ pF}/\mu\text{m}^2$ [83]), the transepithelial potential satisfies $\Delta\phi = \Delta\sigma/C$, where $\Delta\sigma$ is the difference of charge density across the epithelium. Assuming that ions equilibrate quickly in the lumen, excess freely-diffusing charges in the lumen will be located in a thin layer covering the epithelium with a typical thickness given by the Debye-Hückel length scale ℓ_{DH} (see Box “Interaction of charged surfaces”); giving rise to the charge difference $\Delta\sigma$. Assuming also that the solution in the basal side is electrically neutral, $\Delta\sigma = V \sum_i q_i^l c_i^l/A$ with V and A the volume and surface area of the lumen.

The cross-coupling coefficients $\lambda_{w,i}$, $\lambda_{i,w}$ and $\lambda_{i,j}$, which satisfy $\lambda_{i,w} = \lambda_{w,i}\bar{c}_i/kT$ and $\lambda_{i,j}\bar{c}_j = \lambda_{j,i}\bar{c}_i$ due to the underlying Onsager reciprocal relations, stem from

passive interactions between water and ions and different ions across the monolayer. Cross-couplings between ion transport characterised by the coefficients $\lambda_{i,j}$ can be attributed to cotransporters which transport several species simultaneously across the cell membrane. Symporters such as NKCC1 can use favorable differences in chemical potential of some of the transported species (e.g. Na^+ in the case of NKCC1) to transport other molecules against their electrochemical potential (e.g. Cl^- and K^+ in the case of NKCC1 [84]). The coefficients $\lambda_{i,j}$ therefore effectively appear in models for ion transport across the monolayer which incorporate fluxes due to different symporters, whose rate of transport is driven by concentration differences of transported ions [85, 86]. The coefficients $\lambda_{w,i}$ give rise to the osmotic Staverman’s reflection coefficients, $r_i = 1 - \lambda_{w,i}/(kT\lambda_w)$ [67, 87]. For fully impermeable species which do not cross the epithelium, $\lambda_i = \lambda_{i,w}/\lambda_{w,i} = 0$ and the corresponding reflection coefficient $r_i = 1$. What is the possible origin of the cross coupling coefficients $\lambda_{i,w}$, $\lambda_{w,i}$, in epithelial monolayers? In *Xenopus* oocytes the Na^+ /glucose symporter has been shown to cotransport water [70] which leads to a nonzero λ_{w,Na^+} coefficient. Water can also in principle be dragged due to paracellular flows of solutes across paracellular junctions [88]. In the case of an uneven coupling between water with anions and cations, for instance because of symporters cotransporting water, or because some ionic species bind more strongly to the cell surface than others, the theory predicts an electro-osmotic coupling, i.e. a water flux j_w driven by a transepithelial potential $\Delta\phi$, in the absence of an osmotic pressure difference [72]. In the corneal endothelium, a coupling between water flows and ionic current has been measured with a magnitude $2.4 \text{ }\mu\text{m}\cdot\text{cm}^2/(\text{h } \mu\text{Amp})$ [69]. Given that the electric resistance of the endothelium $\omega = 20 \text{ }\Omega\cdot\text{cm}^2$, this leads to a measure for $\lambda_{w,i}q_i\bar{c}_i/kT$ that can be used to obtain $\lambda_{w,\text{Na}^+} = 1.4 \cdot 10^{-8} \text{ }\mu\text{m}^4/\text{s}$. For comparison, we can discuss the electro-osmotic flux that arises in the intercellular-space as a response to an electric field, triggering the motion of the layer of freely diffusing ions located near the charged membrane [89]. We assume that an electric field $-\Delta\phi/h_e$ with h_e the tissue apico-basal height, oriented along the apico-basal axis, is present in the intercellular space. We also assume that cell membranes lining the intercellular space are charged, with the charge characterised by the cell membrane zeta-potential ζ ; and that Na^+ is providing the counterions. The electric field then gives rise to a plug flow in the intercellular space, whose velocity is given by the Helmholtz-Smoluchowski formula, $v \sim e\zeta/(\eta_w h_e)\Delta\phi$, with η_w the water viscosity [30]. The corresponding flux of water across the epithelium is $j_w = \phi_{\text{LIS}}v$ with ϕ_{LIS} the volumic fraction of intercellular space in the tissue. Identification with Eq. (3) then gives $\lambda_{w,\text{Na}^+} \sim -2\ell_{\text{DH}}^2 e\zeta/(\eta_w h_e)\phi_{\text{LIS}}$. With $\eta_w = 10^{-3} \text{ Pa}\cdot\text{s}$, $\zeta = -30 \text{ mV}$ [90], $h_e = 10 \text{ }\mu\text{m}$, $\ell_{\text{DH}} \simeq 1 \text{ nm}$ and $\phi_{\text{LIS}} = 10^{-2}$, one finds indeed a comparable value of $\lambda_{w,\text{Na}^+} \sim 10^{-8} \text{ }\mu\text{m}^4/\text{s}$. With these numbers, a difference of electric potential of 1 mV can elicit

a water flow with velocity $0.02 \mu\text{m/s}$ [28]; a sufficiently large number compared to reported flows in lumen formation of $\sim \mu\text{m/h}$ for this effect to play a role in practice. Whether or not these cross-coupling effects contribute to water pumping might depend on the type of epithelium [72].

The differences in ionic concentrations across the epithelium that drive passive water flows given by the mechanisms described in the previous paragraphs are set by the effect of ionic pumps, which generate an active flux density j_i^{active} . In the steady state, the total flux $j_i = j_i^{\text{active}} + j_i^{\text{passive}} = 0$. Although numerous pumping mechanisms in epithelial cells have been reported, see [80, 91] for an extensive review, here we describe the main processes leading to active transport of ions across MDCK cysts (Fig. 2b). By hydrolysing ATP, the Na^+/K^+ -ATPase pump transports three Na^+ from the cytoplasm to the interstitial fluid and two K^+ in the opposite direction per cycle with a turnover of the order of 10^2 s^{-1} [80]. The activity of the Na^+/K^+ -ATPase pump, as well as its basolateral distribution following the establishment of the cell apico-basal polarity, is required for lumen formation, e.g. inhibition of the Na^+/K^+ -ATPase pump by ouabain blocks lumen formation [6]. The Na^+/K^+ -ATPase pump generates an electrochemical driving force for the entry of Na^+ into the cell, which through symporters such as NKCC1 leads to the import of other ions such as Cl^- [84]. Chloride is then exported to the lumen through channels such as CaCC or CFTR. Inhibition/activation of these channels leads to decreased/increased lumen size [6, 92]. Altogether, this leads to ionic flux of Cl^- across the monolayer which is indirectly actively driven. In turn, this generates an electrochemical gradient across the epithelium which draws a passive paracellular flow of Na^+ , i.e. across the intercellular space, into the lumen.

We now discuss how the previous ingredients can be used to derive a simple picture for the growth of a spherical lumen. For simplicity, we do not take into account here the different passive cross-coupling terms between water flux and ion chemical potential difference, and conversely between ion fluxes and water chemical potential difference. For a spherical lumen of radius R , Eqs. (3) and (4) give for the rate of change of the radius R and lumen concentration c_i ,

$$\begin{aligned} \dot{R} &= \lambda_w [\Delta\Pi - \Delta P], \\ \frac{R}{3} \dot{c}_i &= -\dot{R}c_i - \lambda_i \left[\Delta c_i + \frac{q_i \bar{c}_i}{kT} \Delta\phi \right] + j_i^{\text{active}}, \end{aligned} \quad (10)$$

where $\Delta\phi = R/(3C) \sum_i q_i \Delta c_i$, $\Delta\Pi = kT \sum_i \Delta c_i$ and the difference of hydraulic pressure satisfies Laplace's law $\Delta P = 2t/R$ with t the surface tension in the monolayer. In Eq. (10) we have made the approximation that the volume change in the lumen is entirely due to the water flux across the epithelium. For simplicity, we can consider j_i^{active} to be constant. Assuming a density of $10^3 - 10^4 \mu\text{m}^{-2}$ Na^+/K^+ -ATPase pumps [93] with a turnover of $10^2 - 10^4 \text{ s}^{-1}$ [80], $j_i^{\text{active}} \sim 10^5 - 10^8 \mu\text{m}^{-2} \text{ s}^{-1}$, whose

lower range is consistent with pumping rates measured across MDCK monolayers [51, 56, 94], as well as net Na^+ fluxes measured across the rabbit corneal endothelium [95]. Similar equations have been used in recent studies [24, 26, 28, 96], although the transepithelial potential is not always explicitly considered.

To clarify the discussion, we consider a simple case of a pump-leak mechanism where an anion with charge $-e$ and concentration c_0 is pumped towards the lumen with an active flux density j^{active} , while a corresponding cation with charge $+e$ with concentration c_+ diffuses through the epithelium passively. The external concentrations are also taken to be fixed, $c_+^o = c_-^o = c_0$; and the permeability of the epithelium to both ions taken to be equal, $\lambda = \lambda_+ = \lambda_-$. At low epithelial capacitance C and for constant lumen radius R , the steady-state concentration differences are $\Delta c_+ = \Delta c_- = j^{\text{active}}/(2\lambda)$ and the transepithelial potential $\Delta\phi = (\Delta c_+/\bar{c})(kT/e)$ ($\bar{c} \simeq c_0$ here as we assume small concentration differences). In this expression, kT/e is a characteristic electric potential which is about 27 mV, an order of magnitude comparable to measured transepithelial potentials. The equilibrium radius for the lumen is then given by the balance of hydrostatic and osmotic pressure, giving $2t/R = kTj^{\text{active}}/\lambda$. With the ranges discussed above $j^{\text{active}} = 10^5 - 10^8 \mu\text{m}^{-2} \cdot \text{s}^{-1}$ and $\lambda = 3 \times 10^{-2} - 3 \mu\text{m} \cdot \text{s}^{-1}$, this gives Δc ranging from 0.07 mM to 7×10^3 mM - values in the middle of this range are consistent with physiological concentration of ions of ~ 100 mM [30]. Depending on the constitutive law for the monolayer tension and dependency of the active flux density j^{active} on the lumen size, one expects the equilibrium lumen size given by the radius $2t\lambda/(kTj^{\text{active}})$ to be stable or unstable: e.g. if the epithelial tension t is independent of strain and the active flux density j^{active} is constant, the equilibrium state is unstable as an increase of the radius leads to a decrease in the hydrostatic pressure and further flow towards the lumen; this point is further discussed in the next section. Elastic stresses in the epithelium would generally tend to stabilise the lumen [28], as can be seen from Eq. (10). Indeed, considering an elastic epithelium with surface tension given by $t = t_0 + 2K\delta R/R_0$ with t_0 and R_0 the steady-state epithelial tension and radius, δR a perturbation of the radius and K the epithelial area elastic modulus, the pressure change in the lumen due to a change in epithelium radius is given by $\delta P = 2[2K - t_0]\delta R/R_0^2$ which is stabilising for $K > t_0/2$. Physically, an increase in lumen radius leads to a positive tension in the epithelium due to elastic stretching, increasing the excess hydrostatic pressure in the lumen and favouring fluid expulsion.

The steady-state relations obtained above indicate that lumens do not need to be perfectly sealed to grow: the balance between the active pumping density flux j^{active} and leakage with rate λ can set up a difference of concentration gradient allowing for lumen expansion. Indeed, pumping of ions within a forming cavity leads to a positive osmotic pressure which favours the growth of

the cavity and counteracts its tendency to close due to the cortical surface tension [21]. Leakage of ions is opposing the growth of the cavity, due to the reduction of the osmotic pressure associated to ion loss. A dynamic balance between these effects implies that for any value of the leakage magnitude, a threshold rate of pumping can compensate and ensure that the cavity is growing [21].

In a dynamically growing lumen, the luminal concentrations are also changing by dilution, due to incoming water fluxes. Keeping explicit forms for the fluxes j_i and j_w , the change of concentration in the lumen can indeed be written:

$$\frac{R}{3} \dot{c}_i^l = j_i - j_w c_i^l, \quad (11)$$

such that a constant luminal concentration c_i^l can be maintained during lumen expansion if the water and solute fluxes balance according to $j_i = c_i^l j_w$ [28]. If the role of the hydrostatic pressure difference ΔP can be neglected compared to the osmotic pressure difference $\Delta \Pi$ and the influx of solute j_i is constant, the model then predicts the relaxation to a constant solute concentration in the lumen, $c_i^l = j_i / j_w$ and convergence to a linear radius increase $dR/dt = j_w$.

In this discussion we have incorporated a simple description of electric effects. A recent theoretical work has studied a possible role in lumen formation for flexoelectricity, the establishment of an electric current in the tissue that is sensitive to tissue curvature [97]. Flexoelectricity can lead to an effective negative surface tension of the inner interface of the tissue facing the lumen, generally favoring growth and allowing for lumen nucleation, even when the osmotic pressure difference is unfavorable to lumen expansion.

II. LUMEN INTERACTIONS: PHYSICS OF HYDRAULIC FLOWS IN TISSUES

We now discuss interactions of several lumens in biological tissues. As discussed in the introduction, large lumen formation can occur through intermediate steps involving the growth and fusion of multiple smaller micro-lumens. In recent years several key points on the physics of lumen communication have been made. If lumens are enclosed by cellular interfaces under tension due to the action of the myosin cytoskeleton [73], this results in an excess hydrostatic pressure in the lumen given by the law of Laplace, $\Delta P = 2t/R$, with t the epithelial surface tension and R the radius of curvature. Such configuration is fundamentally unstable if the tension t is constant (Fig. 3a): indeed a reduction of the radius of curvature R leads to a higher hydrostatic pressure difference ΔP , which favours expulsion of the fluid out of the cavity and further reduction of the radius R . If the osmotic pressure difference between the lumen and the extracellular space, $\Delta \Pi$ is constant, a critical radius $R^* = 2t/\Delta \Pi$ determines whether the lumen collapses (for $R < R^*$) and

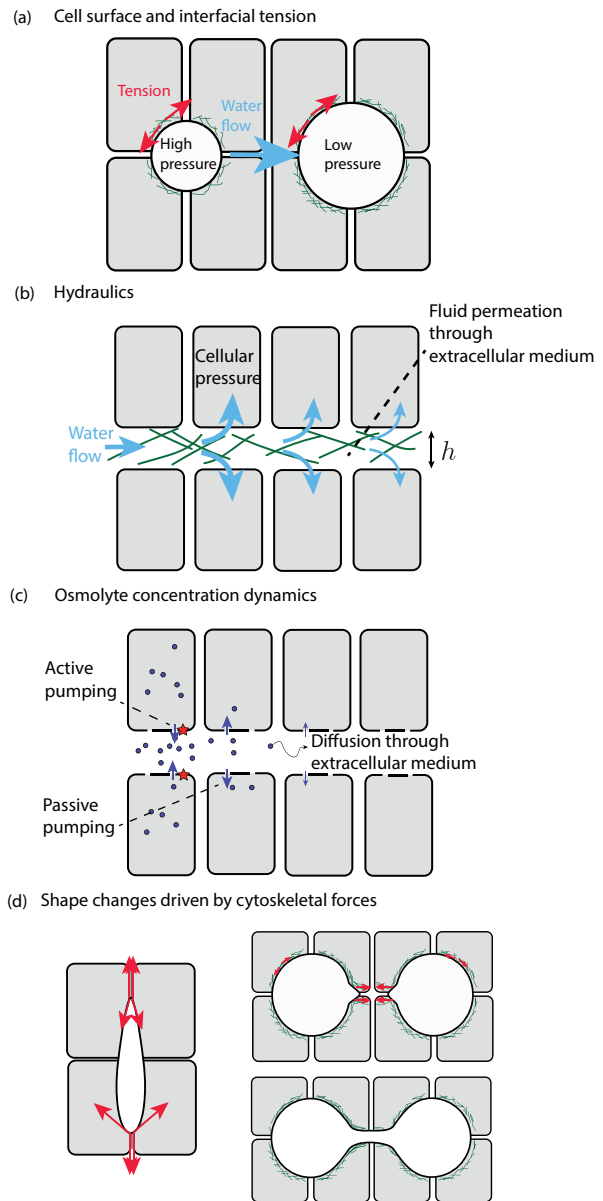


FIG. 3: Interactions of several lumens. (a) Imbalance of lumen hydrostatic pressure can drive fluid flows. In the case of spherical lumens under constant surface tension, water flows from smaller lumens towards larger lumen. (b) Fluid flows and pressure gradients depend on fluid permeation through the extracellular space and through cell membranes. (c) Gradient of extracellular osmolyte concentration depend on their diffusion through the interstitial space, as well as active and passive pumping through cellular membranes. (d) Lumen shapes can depend on gradients of cortical tensions [45]. Lumen coalescence can be driven by cellular contractions and rearrangements.

expands indefinitely (for $R > R^*$). By contrast, if the total osmolyte number is fixed inside the lumen, osmotic pressure provides a stabilising effect as constriction of the lumen leads to an increase in osmolyte concentration, and an increase in the lumen osmotic pressure difference $\Delta \Pi$

which restores the lumen initial size.

Because of this fundamental instability, when several spherical cavities subjected to equal surface tension are brought into contact, a flow arises directed from smaller cavities towards larger cavities (Fig. 3a). In binary mixtures that phase separate, a similar physical instability gives rise to Ostwald ripening. In this dynamic process, small droplets of one of the mixture component progressively coarsen, through a diffusive flux which favours the growth of bigger droplets at the expense of smaller droplets [98]. As droplets coarsen, the interfacial energy of the mixture is reduced, such that the end result, in a finite system, is the thermodynamically stable state of a single droplet rich in one component, surrounded by a medium rich in the second component. Similarly, one would expect such a process of lumen coarsening in a tissue to eventually result in a single lumen. This is indeed the dynamics that has been experimentally observed in mouse blastocysts [9]. In line with the picture of water flowing from microlumens of high pressure to microlumens of lower pressures, the position of the emerging single lumen can be biased experimentally by mixing cells with higher and lower surface tension, through knock out of Myh9 [9]; as expected the cells surrounding the winning lumen are more likely to have a lower tension. A characteristic scaling law of growth controls Ostwald ripening, such that the mean droplet radius R increases with time t as $R \sim t^{\frac{1}{3}}$ for diffusion-limited growth [99]. It is unclear if a similar scaling relation can also be determined in the process of lumen fusion and coarsening.

How does water flow in response to gradients of hydrostatic pressure? It seems reasonable to assume that water flows in the extracellular space of a tissue according to Darcy's law, such that a gradient of hydrostatic pressure in the extracellular fluid, P^f , drives a flow of the extracellular fluid \mathbf{v}^f , according to the relation [100]:

$$\nabla P^f + \kappa(\mathbf{v}^f - \mathbf{v}^c) = 0, \quad (12)$$

where \mathbf{v}^c is the coarse-grained cell velocity in the tissue, and κ is a permeation constant. The Darcy equation above describes flows in porous media; here the coefficient of permeability κ is associated to flow of the interstitial fluid through the extracellular matrix or through intercellular spaces in the tissue. If the extracellular fluid is flowing with viscosity η_w in a extracellular filament networks with filaments separated by a distance δ , the permeation constant is $\kappa \sim 32\eta_w/\delta^2$ ([101], we added a numerical prefactor here corresponding to Poiseuille flow in a tube of radius $\delta/2$). The typical time scale for pressure equilibration between lumens is then $\tau \sim R^2\ell\kappa/(2t) \sim 16R^2\ell\eta_w/(t\delta^2)$; with ℓ a characteristic distance between lumens. With the viscosity of water $\eta_w = 10^{-3}\text{Pa}\cdot\text{s}$, $t \sim 100 \text{ pN}\cdot\mu\text{m}^{-1}$ [73], $\delta \sim 50\text{nm}$ [102], and $R = \ell = 20 \mu\text{m}$, this gives $\tau \sim 500 \text{ s}$. This timescale is roughly in line with the duration of lumen coarsening observed in the formation of the mouse blastocoele [9]. We note however that the estimate for this timescale is highly sensitive to the actual value of the extracellu-

lar matrix mesh size. In addition, other dissipative processes, for instance associated to cellular deformations and rearrangements, might also limit the deformation of lumens in morphogenetic processes.

This analysis of flow between lumens is modified if one takes into account that water can also flow across the cell membrane ([21], Fig. 3b). The competing processes of flow through the intercellular space and through the cell membrane give rise to a characteristic screening length,

$$\xi_w = \sqrt{\frac{h}{\lambda_m\kappa}}, \quad (13)$$

with h the width of the extracellular space, and λ_m the membrane permeability to water. Above this length-scale, extracellular flows are screened by absorption of the fluid into the surrounding cells. What is the order of magnitude of this length scale? With $h = 0.1 \mu\text{m}$ and $\lambda_m \sim 0.7 \times 10^{-7} \mu\text{m}\cdot\text{s}^{-1}\cdot\text{Pa}^{-1}$ (discussed in section I), one finds $\xi = 300 \mu\text{m}$. This relatively large length scale (~ 30 cell lengths, taking a typical cell diameter of $10 \mu\text{m}$) indicates that hydraulic communication between lumens can be relevant to their dynamics. As noted above, the permeation constant κ however varies strongly with the mesh size δ , and the length scale h for the dimension of the intercellular space is also likely to vary significantly, so that the precise value of the length scale ξ_w could vary between experimental systems.

What is the dynamics of osmolytes (Fig. 3c)? Osmolytes passively flow in the extracellular space and a diffusion flux should occur to balance concentration in different microlumens. Here as well such diffusive fluxes are screened by exchange with the intracellular space, through pumping of osmolytes across the cell membranes. This length scale can be written [21]

$$\xi_i = \sqrt{\frac{Dh}{\lambda_i}}, \quad (14)$$

with D the diffusion constant of osmolytes in the extracellular medium, and λ_{osm} the membrane osmolyte permeability. A typical diffusion constant for ions in a tissue is $D \sim 500 \mu\text{m}^2\cdot\text{s}^{-1}$ [103]. Taking again $h = 0.1 \mu\text{m}$ and $\lambda_i = 3 \times 10^{-2} - 3 \mu\text{m}/\text{s}$, one finds $\xi_i \sim 4 - 40 \mu\text{m}$. This length scale arises from a competition between diffusion in the extracellular space and reabsorption in the cell. In a thick epithelium, this length scale could limit paracellular ion exchange across the epithelium, as ions would diffuse into the cells before crossing the epithelium. This length scale also determines, in principle, whether neighbouring microlumens share solutes that are pumped towards the lumens.

The length-scale involved in Eq. 14 arises from a similar competition of processes to the diffusion-degradation model involved in morphogen gradient formation and spread, determining a patterning length scale $\sqrt{D/k}$ with D the morphogen diffusion constant and k an effective degradation rate [104]. In Eq. (14), osmolytes are assumed to flow passively through the membrane instead

of binding to cell membrane receptors and being internalised. In both cases, this length-scale determine the range of cell-cell communication occurring through diffusible molecules. The presence of the h factor in Eq. (14) indicates that the length scale increases with the size of the intercellular space. Interestingly microlumens forming in the zebrafish lateral line primordium have been called “luminal hubs”, as cells sharing a common lumen exhibits a coordinated behaviour as a result of FGF concentrating specifically in the shared lumen [43].

The shape of forming lumens is not necessarily spherical (Fig. 3d): indeed due to the Young-Dupré force balance equation at the junctions between several cells, the interface surfaces can in principle deform away from a spherical shape to establish force balance at the cellular junctions. In liver cells cultured *in vitro*, early lumens open preferentially towards the tissue interface with the free medium, away from the extracellular matrix [45]. This asymmetric lumen growth process has been suggested to arise from differences in junctional tensions across cellular junctions. Differences in interfacial tension could also in principle drive lumen fusion, bringing lumens into contact for them to undergo coalescence by contact (Fig. 3d). During zebrafish gut development, the intestinal tube forms in several stages, starting with the initiation of multiple small lumens within a solid rod of endodermal cells, followed by lumen fusion and resolution [14]. This fusion process could occur through de-adhesion of cellular interfaces in the bridge connecting adjacent lumens, or through contraction of the cellular interfaces participating to the bridge [14]. More generally, coalescence by direct contact (Fig. 3d) or “ripening” based on fluid flows between lumens (Fig. 3a) are two processes that could be responsible for lumen fusion, separately or

in combination.

III. CONCLUSION

The physics of lumen formation involves multiple length scales and a complex interplay of hydraulic flows, cell mechanics, and electric and electro-osmotic effects. This topic has attracted significant interest in recent years, as it is becoming evident that the dynamics and mechanics of lumen formation plays a key role in morphogenetic processes during development. Stem cells aggregate have the ability to spontaneously form a lumen, indicating that lumen formation is a fundamental self-organising ability of cell aggregates. How this self-organisation occurs is a key question at the interface of physics and biology. The interplay of lumen formation with cellular forces and pumping, but also with cell polarity, morphogen gradient and cell signalling, and electric forces and currents leads to a large range of situations and rich physical behaviours.

Acknowledgement

ATS, MKW, and GS acknowledge support from the Francis Crick Institute, which receives its core funding from Cancer Research UK (FC001317), the UK Medical Research Council (FC001317), and the Wellcome Trust (FC001317).

Competing interests

The authors have no competing interests to declare.

-
- [1] Anirban Datta, David M. Bryant, and Keith E. Mostov. Molecular regulation of lumen morphogenesis. *Current Biology*, 21(3):R126–R136, 2011.
 - [2] Sara Sigurbjörnsdóttir, Renjith Mathew, and Maria Leptin. Molecular mechanisms of de novo lumen formation. *Nature Reviews Molecular Cell Biology*, 15(10):665–676, 2014.
 - [3] Adam Navis and Michel Bagnat. Developing pressures: fluid forces driving morphogenesis. *Current Opinion in Genetics and Development*, 32:24–30, 2015.
 - [4] Alex J Blasky, Anthony Mangan, and Rytis Prekeris. Polarized protein transport and lumen formation during epithelial tissue morphogenesis. *Annual review of cell and developmental biology*, 31:575–591, 2015.
 - [5] Adam Navis and Celeste M Nelson. Pulling together: Tissue-generated forces that drive lumen morphogenesis. In *Seminars in cell & developmental biology*, volume 55, pages 139–147. Elsevier, 2016.
 - [6] Michel Bagnat, Isla D. Cheung, Keith E. Mostov, and Didier Y.R. Stainier. Genetic control of single lumen formation in the zebrafish gut. *Nature Cell Biology*, 9(8):954–960, 2007.
 - [7] Laura Anne Lowery and Hazel Sive. Initial formation of zebrafish brain ventricles occurs independently of circulation and requires the *nagie oko* and *snakehead/atp1a1a.1* gene products. *Development*, 132(9):2057–2067, 2005.
 - [8] Jingjing Zhang, Jörg Piontek, Hartwig Wolburg, Christian Piehl, Martin Liss, Cécile Otten, Annabel Christ, Thomas E Willnow, Ingolf E Blasig, and Salim Abdelilah-Seyfried. Establishment of a neuroepithelial barrier by *claudin5a* is essential for zebrafish brain ventricular lumen expansion. *Proceedings of the National Academy of Sciences*, 107(4):1425–1430, 2010.
 - [9] Julien G. Dumortier, Mathieu Le Verge-Serandour, Anna Francesca Tortorelli, Annette Mielke, Ludmilla De Plater, Hervé Turlier, and Jean Léon Maître. Hydraulic fracturing and active coarsening position the lumen of the mouse blastocyst. *Science*, 365(6452):465–468, 2019.
 - [10] Agnik Dasgupta, Matthias Merkel, Madeline J Clark, Andrew E Jacob, Jonathan Edward Dawson, M Lisa Manning, and Jeffrey D Amack. Cell volume changes contribute to epithelial morphogenesis in zebrafish kupf-

- fer's vesicle. *Elife*, 7:e30963, 2018.
- [11] Pavel I Nedvetsky, Elaine Emmerson, Jennifer K Finley, Andreas Ettinger, Noel Cruz-Pacheco, Jan Prochazka, Candace L Haddox, Emily Northrup, Craig Hodges, Keith E Mostov, et al. Parasympathetic innervation regulates tubulogenesis in the developing salivary gland. *Developmental cell*, 30(4):449–462, 2014.
- [12] Ivan Bedzhov and Magdalena Zernicka-Goetz. Self-organizing properties of mouse pluripotent cells initiate morphogenesis upon implantation. *Cell*, 156(5):1032–1044, 2014.
- [13] Marta N. Shahbazi, Agnieszka Jedrusik, Sanna Vuoristo, Gaele Recher, Anna Hupalowska, Virginia Bolton, Norah M. E. Fogarty, Alison Campbell, Liani G. Devito, Dusko Ilic, Yakoub Khalaf, Kathy K. Niakan, Simon Fishel, and Magdalena Zernicka-Goetz. Self-organization of the human embryo in the absence of maternal tissues. *Nature Cell Biology*, 18(6):700–8, 2016.
- [14] Ashley L. Alvers, Sean Ryan, Paul J. Scherz, Jan Huisken, and Michel Bagnat. Single continuous lumen formation in the zebrafish gut is mediated by smoothed-dependent tissue remodeling. *Development (Cambridge)*, 141(5):1110–1119, 2014.
- [15] Jennifer Zenker, Melanie D White, Maxime Gasnier, Stephanie Bissiere, Nicolas Plachta, Jennifer Zenker, Melanie D White, Maxime Gasnier, Yanina D Alvarez, Hui Yi, Grace Lim, and Stephanie Bissiere. Expanding Actin Rings Zipper the Mouse Embryo for Blastocyst Formation. *Cell*, 173:776–791, 2018.
- [16] Magdalena Zernicka-Goetz. Cleavage pattern and emerging asymmetry of the mouse embryo. *Nature Reviews Molecular Cell Biology*, 6(12):919–928, 2005.
- [17] Stephen R. Frankenberg, Flavia R.O. de Barros, Janet Rossant, and Marilyn B. Renfree. The mammalian blastocyst. *Wiley Interdisciplinary Reviews: Developmental Biology*, 5(2):210–232, 2016.
- [18] Connie C. Wong, Kevin E. Loewke, Nancy L. Bossert, Barry Behr, Christopher J. De Jonge, Thomas M. Baer, and Renee A.Reijo Pera. Non-invasive imaging of human embryos before embryonic genome activation predicts development to the blastocyst stage. *Nature Biotechnology*, 28(10):1115–1121, 2010.
- [19] Yusuke Marikawa and Vernadeth B. Alarcon. Creation of trophoctoderm, the first epithelium, in mouse preimplantation development. *Results and Problems in Cell Differentiation*, 55:165–184, 2012.
- [20] Chii J. Chan and Takashi Hiiragi. Integration of luminal pressure and signalling in tissue self-organization. *Development (Cambridge)*, 147(5):1–10, 2020.
- [21] Sabyasachi Dasgupta, Kapish Gupta, Yue Zhang, Virgile Viasnoff, and Jacques Prost. Physics of lumen growth. *Proceedings of the National Academy of Sciences of the United States of America*, 115(21):E4751–E4757, 2018.
- [22] Aki Manninen. Epithelial polarity - Generating and integrating signals from the ECM with integrins. *Experimental Cell Research*, 334(2):337–349, 2015.
- [23] Hiroaki Okuyama, Jumpei Kondo, Yumi Sato, Hiroko Endo, Aya Nakajima, Jose M. Piulats, Yasuhiko Tomita, Takeshi Fujiwara, Yu Itoh, Akira Mizoguchi, Masayuki Ohue, and Masahiro Inoue. Dynamic change of polarity in primary cultured spheroids of human colorectal adenocarcinoma and its role in metastasis. *American Journal of Pathology*, 186(4):899–911, 2016.
- [24] Chii Jou Chan, Maria Costanzo, Teresa Ruiz-Herrero, Gregor Mönke, Ryan J. Petrie, Martin Bergert, Alba Diz-Muñoz, L. Mahadevan, and Takashi Hiiragi. Hydraulic control of mammalian embryo size and cell fate. *Nature*, 571(7763):112–116, 2019.
- [25] C Fütterer, C Colombo, F Jülicher, and A Ott. Morphogenetic oscillations during symmetry breaking of regenerating hydra vulgaris cells. *EPL (Europhysics Letters)*, 64(1):137, 2003.
- [26] Teresa Ruiz-Herrero, Kévin Alessandri, Basile V. Gurchenkov, Pierre Nassoy, and L. Mahadevan. Organ size control via hydraulically gated oscillations. *Development (Cambridge)*, 144(23):4422–4427, 2017.
- [27] Ian A. Swinburne, Kishore R. Mosaliganti, Srigokul Upadhyayula, Tsung Li Liu, David G.C. Hildebrand, Tony Y.C. Tsai, Anzhi Chen, Ebaa Al-Obeidi, Anna K. Fass, Samir Malhotra, Florian Engert, Jeff W. Lichtman, Tomas Kirchhausen, Eric Betzig, and Sean G. Megason. Lamellar projections in the endolymphatic sac act as a relief valve to regulate inner ear pressure. *eLife*, 7:1–34, 2018.
- [28] Kishore R. Mosaliganti, Ian A. Swinburne, Chon U. Chan, Nikolaus D. Obholzer, Amelia A. Green, Shreyas Tanksale, L. Mahadevan, and Sean G. Megason. Size control of the inner ear via hydraulic feedback. *eLife*, 8:1–30, 2019.
- [29] Véronique Gebala, Russell Collins, Ilse Geudens, Li-Kun Phng, and Holger Gerhardt. Blood flow drives lumen formation by inverse membrane blebbing during angiogenesis in vivo. *Nature cell biology*, 18(4):443–450, 2016.
- [30] Hans-Jürgen Butt, Karlheinz Graf, and Michael Kappl. *Physics and chemistry of interfaces*. John Wiley & Sons, 2013.
- [31] Ram M. Adar, Tomer Markovich, Amir Levy, Henri Orland, and David Andelman. Dielectric constant of ionic solutions: Combined effects of correlations and excluded volume. *Journal of Chemical Physics*, 149(5), 2018.
- [32] T. D. Perez and W. J. Nelson. Cadherin Adhesion: Mechanisms and Molecular Interactions. *Handbook of Experimental Pharmacology*, 5(165):3–21, 2004.
- [33] Porntula Panorchan, Melissa S Thompson, Kelly J Davis, Yiider Tseng, Konstantinos Konstantopoulos, and Denis Wirtz. Single-molecule analysis of cadherin-mediated cell-cell adhesion. *Journal of cell science*, 119(1):66–74, 2006.
- [34] P. Katsamba, K. Carroll, G. Ahlsen, F. Bahna, J. Vendome, S. Posy, M. Rajebhosale, S. Price, T. M. Jessell, A. Ben-Shaul, L. Shapiro, and Barry H. Honig. Linking molecular affinity and cellular specificity in cadherin-mediated adhesion. *Proceedings of the National Academy of Sciences of the United States of America*, 106(28):11594–11599, 2009.
- [35] The podocalyxin charge was estimated using the amino acid sequence from <https://www.uniprot.org/uniprot/o00592>, and the protein charge calculator at <https://pepcalc.com/protein-calculator.php>.
- [36] D. Kerjaschki, A. T. Vernillo, and M. G. Farquhar. Reduced sialylation of podocalyxin - The major sialoprotein of the rat kidney glomerulus - in aminonucleoside nephrosis. *American Journal of Pathology*, 118(3):343–349, 1985.
- [37] A Varki, R D Cummings, and J D Esko. Essentials of

- Glycobiology, Chapter 14. In *Essentials of Glycobiology*. Cold Spring Harbor Laboratory Press, 2nd edition, 2009.
- [38] Boris Strilić, Tomáš Kučera, Jan Eglinger, Michael R Hughes, Kelly M McNagny, Sachiko Tsukita, Elisabetta Dejana, Napoleone Ferrara, and Eckhard Lammert. The molecular basis of vascular lumen formation in the developing mouse aorta. *Developmental cell*, 17(4):505–515, 2009.
- [39] Boris Strilić, Jan Eglinger, Michael Krieg, Martin Zeeb, Jennifer Axnick, Pavel Babál, Daniel J. Müller, and Eckhard Lammert. Electrostatic cell-surface repulsion initiates lumen formation in developing blood vessels. *Current Biology*, 20(22):2003–2009, 2010.
- [40] T. Takeda, W. Y. Go, R. A. Orlando, and M. G. Farquhar. Expression of podocalyxin inhibits cell-cell adhesion and modifies junctional properties in Madin-Darby canine kidney cells. *Molecular Biology of the Cell*, 11(9):3219–3232, 2000.
- [41] Julie S Nielsen and Kelly M McNagny. Novel functions of the cd34 family. *Journal of cell science*, 121(22):3683–3692, 2008.
- [42] Julie S Nielsen, Marcia L Graves, Shierley Chelliah, A Wayne Vogl, Calvin D Roskelley, and Kelly M McNagny. The cd34-related molecule podocalyxin is a potent inducer of microvillus formation. *PLoS one*, 2(2):e237, 2007.
- [43] Sevi Durdu, Murat Iskar, Celine Revenu, Nicole Schieber, Andreas Kunze, Peer Bork, Yannick Schwab, and Darren Gilmour. Luminal signalling links cell communication to tissue architecture during organogenesis. *Nature*, 515(7525):120–124, 2014.
- [44] Allyson Quinn Ryan, Chii Jou Chan, François Graner, and Takashi Hiragi. Lumen expansion facilitates epiblast-primitive endoderm fate specification in the mouse blastocyst formation. *Developmental Cell*, page 575282, 2019.
- [45] Qiushi Li, Yue Zhang, Perrine Pluchon, Jeffrey Robens, Keira Herr, Myriam Mercade, Jean-Paul Thiery, Henry Yu, and Virgile Viasnoff. Extracellular matrix scaffolding guides lumen elongation by inducing anisotropic intercellular mechanical tension. *Nature Cell Biology*, 18(3):311–318, 2016.
- [46] James A. McAteer, Andrew P. Evan, Ellen E. Vance, and Kenneth D. Gardner. MDCK cysts: An in vitro model of epithelial cyst formation and growth. *Journal of Tissue Culture Methods*, 10(4):245–248, 1986.
- [47] ALLAN Z Wang, GEORGE K Ojakian, and W JAMES Nelson. Steps in the morphogenesis of a polarized epithelium. i. uncoupling the roles of cell-cell and cell-substratum contact in establishing plasma membrane polarity in multicellular epithelial (mdck) cysts. *Journal of cell science*, 95(1):137–151, 1990.
- [48] Wei Yu, Anirban Datta, Pascale Leroy, Lucy Erin O’Brien, Grace Mak, Tzuyu Shuh Jou, Karl S. Matlin, Keith E. Mostov, and Mirjam M.P. Zegers. β 1-integrin orients epithelial polarity via Rac1 and laminin. *Molecular Biology of the Cell*, 16(2):433–445, 2005.
- [49] Wei Yu, Annette M. Shewan, Paul Brakeman, Dennis J. Eastburn, Anirban Datta, David M. Bryant, Qi Wen Fan, William A. Weiss, Mirjam M.P. Zegers, and Keith E. Mostov. Involvement of RhoA, ROCK I and myosin II in inverted orientation of epithelial polarity. *EMBO Reports*, 9(9):923–929, 2008.
- [50] David M. Bryant, Anirban Datta, Alejo E. Rodríguez-Fraticelli, Johan PeräCurrency Signnen, Fernando Martín-Belmonte, and Keith E. Mostov. A molecular network for de novo generation of the apical surface and lumen. *Nature Cell Biology*, 12(11):1035–1045, 2010.
- [51] M Cerejido, J Ehrenfeld, S Fernández-Castelo, and I Meza. Fluxes, junctions, and blisters in cultured monolayers of epithelioid cells (MDCK). *Ann. N. Y. Acad. Sci.*, 372:422–441, 1981.
- [52] C Tanner, D A Frambach, and D S Misfeldt. Transepithelial transport in cell culture. A theoretical and experimental analysis of the biophysical properties of domes. *Biophys. J.*, 43(2):183–190, August 1983.
- [53] S Fernández-Castelo, J J Bolívar, R López-Vancell, G Beaty, and M Cerejido. Ion Transport in MDCK Cells. In Mary Taub, editor, *Tissue Culture of Epithelial Cells*, pages 37–50. Springer US, Boston, MA, 1985.
- [54] M M Timbs and K R Spring. Hydraulic properties of MDCK cell epithelium. *J. Membr. Biol.*, 153(1):1–11, September 1996.
- [55] Laura Casares, Romaric Vincent, Dobryna Zalvidea, Noelia Campillo, Daniel Navajas, Marino Arroyo, and Xavier Trepát. Hydraulic fracture during epithelial stretching. *Nature Materials*, 14(3):343–351, 2015.
- [56] Ernest Latorre, Sohan Kale, Laura Casares, Manuel Gómez-González, Marina Uroz, Léo Valon, Roshna V. Nair, Elena Garreta, Nuria Montserrat, Aránzazu del Campo, Benoit Ladoux, Marino Arroyo, and Xavier Trepát. Active superelasticity in three-dimensional epithelia of controlled shape. *Nature*, 563(7730):203–208, 2018.
- [57] Sarah Ellys Harrison, Berna Sozen, Neophytos Christodoulou, Christos Kyprianou, and Magdalena Zernicka-Goetz. Assembly of embryonic and extraembryonic stem cells to mimic embryogenesis in vitro. *Science*, 356(6334):eaal1810, 2017.
- [58] Berna Sozen, Gianluca Amadei, Andy Cox, Ran Wang, Ellen Na, Sylwia Czukiewska, Lia Chappell, Thierry Voet, Geert Michel, Naihe Jing, David M Glover, and Magdalena Zernicka-goetz. Self-assembly of embryonic and two extra-embryonic stem cell types into gastrulating embryo-like structures. *Nature Cell Biology*, 20(August), 2018.
- [59] Berna Sozen, Andy L. Cox, Joachim De Jonghe, Min Bao, Florian Hollfelder, David M. Glover, and Magdalena Zernicka-Goetz. Self-Organization of Mouse Stem Cells into an Extended Potential Blastoid. *Developmental Cell*, 51(6):698–712.e8, 2019.
- [60] Matteo Mole, Antonia Weberling, Simon Fishel, Magdalena Zernicka-goetz, Antonia Weberling, and Reinhard Fa. Integrin b1 coordinates survival and morphogenesis of the embryonic lineage upon implantation and pluripotency transition. *Cell Reports*, 34, 2021.
- [61] Marta N. Shahbazi, Antonio Scialdone, Natalia Skorupska, Antonia Weberling, Gaelle Recher, Meng Zhu, Agnieszka Jedrusik, Liani G. Devito, Laila Noli, Iain C. MacAulay, Christa Buecker, Yakoub Khalaf, Dusko Ilic, Thierry Voet, John C. Marioni, and Magdalena Zernicka-Goetz. Pluripotent state transitions coordinate morphogenesis in mouse and human embryos. *Nature*, 552(7684):239–243, 2017.
- [62] Denise K Marciano. A holey pursuit: lumen formation in the developing kidney. *Pediatric nephrology*, 32(1):7–20, 2017.

- [63] Senthil K Muthuswamy, Dongmei Li, Sophie Lelievre, Mina J Bissell, and Joan S Brugge. Erbb2, but not erbb1, reinitiates proliferation and induces luminal repopulation in epithelial acini. *Nature cell biology*, 3(9):785–792, 2001.
- [64] Ruba Halaoui, Carlis Rejon, Sudipa June Chatterjee, Joseph Szymborski, Sarkis Meterissian, William J Muller, Atilla Omeroglu, and Luke McCaffrey. Progressive polarity loss and luminal collapse disrupt tissue organization in carcinoma. *Genes & development*, 31(15):1573–1587, 2017.
- [65] Ashna Alladin, Lucas Chaible, Lucia Garcia del Valle, Reither Sabine, Monika Loeschinger, Malte Wachsmuth, Jean Karim Hériché, Christian Tischer, and Martin Jechlinger. Tracking cells in epithelial acini by light sheet microscopy reveals proximity effects in breast cancer initiation. *eLife*, 9:1–20, 2020.
- [66] Neil Ashley, Trevor M. Yeung, and Walter F. Bodmer. Stem cell differentiation and lumen formation in colorectal cancer cell lines and primary tumors. *Cancer Research*, 73(18):5798–5809, 2013.
- [67] O Kedem and A Katchalsky. Permeability of composite membranes. part 1.—electric current, volume flow and flow of solute through membranes. *Transactions of the Faraday Society*, 59:1918–1930, 1963.
- [68] Sybren Ruurds De Groot and Peter Mazur. *Nonequilibrium thermodynamics*. Courier Corporation, 2013.
- [69] J M Sánchez, Y Li, A Rubashkin, P Iserovich, Q Wen, J W Ruberti, R W Smith, D Rittenband, K Kuang, F P J Diecke, and J Fischbarg. Evidence for a Central Role for Electro-Osmosis in Fluid Transport by Corneal Endothelium. *J. Membr. Biol.*, 187(1):37–50, May 2002.
- [70] D D Loo, T Zeuthen, G Chandy, and E M Wright. Cotransport of water by the Na⁺/glucose cotransporter. *Proc. Natl. Acad. Sci. U. S. A.*, 93(23):13367–13370, November 1996.
- [71] K Olbrich, W Rawicz, D Needham, and E Evans. Water permeability and mechanical strength of polyunsaturated lipid bilayers. *Biophysical journal*, 79(1):321–327, 2000.
- [72] Jorge Fischbarg. Fluid transport across leaky epithelia: central role of the tight junction and supporting role of aquaporins. *Physiological reviews*, 90(4):1271–1290, 2010.
- [73] Guillaume Salbreux, Guillaume Charras, and Ewa Paluch. Actin cortex mechanics and cellular morphogenesis. *Trends in Cell Biology*, 22(10):536–545, 2012.
- [74] Vani Narayanan, Laurel E Schappell, Carl R Mayer, Ashley A Duke, Travis J Armiger, Paul T Arsenovic, Abhinav Mohan, Kris N Dahl, Jason P Gleghorn, and Daniel E Conway. Osmotic gradients in epithelial acini increase mechanical tension across e-cadherin, drive morphogenesis, and maintain homeostasis. *Current Biology*, 30(4):624–633, 2020.
- [75] Philippe Marmottant, Abbas Mgharbel, Jos Käfer, Benjamin Audren, Jean-Paul Rieu, Jean-Claude Vial, Boudewijn Van Der Sanden, Athanasius FM Marée, François Graner, and Hélène Delanoë-Ayari. The role of fluctuations and stress on the effective viscosity of cell aggregates. *Proceedings of the National Academy of Sciences*, 106(41):17271–17275, 2009.
- [76] Karine Guevorkian, Marie-Josée Colbert, Mélanie Durth, Sylvie Dufour, and Françoise Brochard-Wyart. Aspiration of biological viscoelastic drops. *Physical review letters*, 104(21):218101, 2010.
- [77] Susanne M Krug, Jörg D Schulzke, and Michael Fromm. Tight junction, selective permeability, and related diseases. *Semin. Cell Dev. Biol.*, 36:166–176, December 2014.
- [78] M Furuse, K Furuse, H Sasaki, and S Tsukita. Conversion of zonulae occludentes from tight to leaky strand type by introducing claudin-2 into Madin-Darby canine kidney I cells. *J. Cell Biol.*, 153(2):263–272, April 2001.
- [79] Henry Sackin and Lawrence G Palmer. Chapter 7 - Electrophysiological Analysis of Transepithelial Transport. In Robert J Alpern, Orson W Moe, and Michael Caplan, editors, *Seldin and Giebisch's The Kidney (Fifth Edition)*, pages 177–216. Academic Press, January 2013.
- [80] Luis Reuss. Chapter 2 - Mechanisms of Ion Transport Across Cell Membranes and Epithelia. In Robert J Alpern and Steven C Hebert, editors, *Seldin and Giebisch's The Kidney (Fourth Edition)*, pages 35–56. Academic Press, San Diego, January 2008.
- [81] Sylvain Bartolami, Sophie Gaboyard, Julie Quentin, Cécile Travo, Mélanie Cavalier, Jacques Barhanin, and Christian Chabbert. Critical roles of transitional cells and Na/K-ATPase in the formation of vestibular endolymph. *J. Neurosci.*, 31(46):16541–16549, November 2011.
- [82] S A Lewis. Everything you wanted to know about the bladder epithelium but were afraid to ask. *Am. J. Physiol. Renal Physiol.*, 278(6):F867–74, June 2000.
- [83] J Wegener, M Sieber, and H J Galla. Impedance analysis of epithelial and endothelial cell monolayers cultured on gold surfaces. *J. Biochem. Biophys. Methods*, 32(3):151–170, July 1996.
- [84] K E Barrett and S J Keely. Chloride secretion by the intestinal epithelium: molecular basis and regulatory aspects. *Annu. Rev. Physiol.*, 62:535–572, 2000.
- [85] BA Benjamin and EA Johnson. A quantitative description of the na-k-2cl cotransporter and its conformity to experimental data. *American Journal of Physiology-Renal Physiology*, 273(3):F473–F482, 1997.
- [86] Elan Gin, Edmund J Crampin, David A Brown, Trevor J Shuttleworth, David I Yule, and James Sneyd. A mathematical model of fluid secretion from a parotid acinar cell. *J. Theor. Biol.*, 248(1):64–80, September 2007.
- [87] AJ Staverman. The theory of measurement of osmotic pressure. *Recueil des Travaux Chimiques des Pays-Bas*, 70(4):344–352, 1951.
- [88] H H Ussing and K Eskesen. Mechanism of isotonic water transport in glands. *Acta Physiol. Scand.*, 136(3):443–454, July 1989.
- [89] Niladri Sarkar, Jacques Prost, and Frank Jülicher. Field induced cell proliferation and death in a model epithelium. *New Journal of Physics*, 21(4):043035, 2019.
- [90] Oxanav V Bondar, DV Saifullina, II Shakhmaeva, II Mavlyutova, and TI Abdullin. Monitoring of the zeta potential of human cells upon reduction in their viability and interaction with polymers. *Acta Naturae*, 4(1(12)), 2012.
- [91] Raymond A Frizzell and John W Hanrahan. Physiology of epithelial chloride and fluid secretion. *Cold Spring Harb. Perspect. Med.*, 2(6):a009563, June 2012.
- [92] Hongyu Li, Iain A Findlay, and David N Sheppard. The relationship between cell proliferation, cl- secretion, and

- renal cyst growth: a study using cftr inhibitors. *Kidney international*, 66(5):1926–1938, 2004.
- [93] H S Ewart and A Klip. Hormonal regulation of the Na(+)-K(+)-ATPase: mechanisms underlying rapid and sustained changes in pump activity. *Am. J. Physiol.*, 269(2 Pt 1):C295–311, August 1995.
- [94] N L Simmons. Ion transport in 'tight' epithelial monolayers of MDCK cells. *J. Membr. Biol.*, 59(2):105–114, April 1981.
- [95] Jong J Lim and Hans H Ussing. Analysis of presteady-state na+ fluxes across the rabbit corneal endothelium. *The Journal of membrane biology*, 65(3):197–204, 1982.
- [96] Elan Gin, Elly M Tanaka, and Lutz Brusch. A model for cyst lumen expansion and size regulation via fluid secretion. *J. Theor. Biol.*, 264(3):1077–1088, June 2010.
- [97] Charlie Duclut, Niladri Sarkar, Jacques Prost, and Frank Jülicher. Fluid pumping and active flexoelectricity can promote lumen nucleation in cell assemblies. *Proceedings of the National Academy of Sciences of the United States of America*, 116(39):19264–19273, 2019.
- [98] Jian Hua Yao, KR Elder, Hong Guo, and Martin Grant. Theory and simulation of ostwald ripening. *Physical review B*, 47(21):14110, 1993.
- [99] JA Marqusee and John Ross. Kinetics of phase transitions: Theory of ostwald ripening. *The Journal of chemical physics*, 79(1):373–378, 1983.
- [100] J Ranft, J Prost, Frank Jülicher, and J.-F. Joanny. Tissue dynamics with permeation. *European Physical Journal E*, 35(46), 2012.
- [101] Pierre-Gilles De Gennes and Pierre-Gilles Gennes. *Scaling concepts in polymer physics*. Cornell university press, 1979.
- [102] Peter D Yurchenco and George C Ruben. Basement membrane structure in situ: evidence for lateral associations in the type iv collagen network. *The Journal of cell biology*, 105(6):2559–2568, 1987.
- [103] M Suenson, DR Richmond, and JB Bassingthwaight. Diffusion of sucrose, sodium, and water in ventricular myocardium. *American Journal of Physiology-Legacy Content*, 227(5):1116–1123, 1974.
- [104] Anna Kicheva, Periklis Pantazis, Tobias Bollenbach, Yannis Kalaidzidis, Thomas Bittig, Frank Jülicher, and Marcos González-Gaitán. Kinetics of morphogen gradient formation. *Science*, 315(5811):521–525, 2007.